NIPES

Journal of Energy Technology and Environment

Journal homepage: www.nipesjournals.org.ng

Bio-Inspired Hydroxyapatite-Chitosan Composite for Enhanced Indigo Blue Dye Removal: Kinetic and Adsorption Optimization Study

O.U.Osazuwa*; E.I. Ehiawaguan, G.J. Obiuwevbi and A.N. Amenaghawon.
Department of Chemical Engineering University of Benin, Benin City, Nigeria
*Corresponding Author: osarieme.osazuwa@uniben.edu.; +234 *8036998276*

Article information

Article History
Received 3 September 2024
Revised 27 October 2024
Accepted 8 November 2024
Available online 19 Dec 2024

Keywords: *Adsorption; Hydroxyapatite; Chitosan; Indigo Blue; Response Surface methodology; Adsorption*

https://doi.org/10.5281/zenodo.14523041.

https://nipes.org

Abstract

The presence of dye molecules in water has a number of negative effects on aquatic and terrestrial animals. This study aimed to synthesize and characterize a composite of hydroxyapatite and chitosan to adsorb Indigo Blue (IB) dye from water, and to optimize its use for the adsorption process using the Response Surface Methodology (RSM) modelling tool. The combination of hydroxyapatite obtained from goat bone and chitosan obtained from periwinkle shell was carried out to enhance the mechanical strength and removal efficiency of the adsorbent. The formulated adsorbent was characterized using BET surface area, SEM-EDX, FTIR, XRD, and XRF techniques. Response surface methodology (RSM) using Box-Behnken Design (BBD) was employed to develop a series of batch-wise adsorption experiments. Findings revealed the R^2 value of the RSM optimization tool to be 0.9854. The optimized conditions used for the adsorption experiments were 180 min, 8.6, 150 mg/L, and 1 g for the adsorption time, pH, dye concentration, and adsorbent dosage, respectively, resulting in an adsorption efficiency of 80.92 %.

1. Introduction

Water, a basic need for all living things on earth, occupies the vast bulk of the planet and accounts for about 71 % of the earth's total surface area [1]. However, freshwater supplies around the world have been threatened due to the rise in contamination from natural or anthropogenic sources [2]. Owing to the importance of water to human activities and environment functions, the United Nations is calling for worldwide access to low-priced potable drinking water by 2030 and this has been listed as one of the Global Sustainable Development Goals (SDGs) [3]. Sectors such as the food packaging, pulp and paper, textile and cosmetics industries, have high utilization of hydrophobic compounds, which are difficult to remove due to their sparing solubility and tendency to bioaccumulate [4]. Literature reports the use of over 8,000 distinct chemicals in producing textiles, with an estimated 5 billion kg of dyes and other chemicals in use today [5].

Natural water bodies remain highly contaminated because the majority of chemicals are not entirely broken down during effluent treatment. Also, weak enforcement of laws concerning wastewater discharge in many countries contributes to this menace. This scenario can be seen playing out in tie and dye Adire production in Nigeria where the effluents usually contain dye and reducing agents

like caustic soda to make the dye molecules soluble in water [6]. To easily remove dye, treatment methods such as coagulation-flocculation [7], biodegradation [8], electrolysis [9], ion exchange [10], and adsorption [11], have been applied. While coagulation and flocculation is relatively cheap, it results in sludge formation [12]. Biodegradation is not very effective in recent times as a result of the non-biodegradability of modern synthetic dyes [13]. Although the electrolysis technique has been found to be efficient, its high-cost implications have limited its application. Adsorption, on the other hand, has shown potential for dye removal from wastewater because of its excellent removal efficiency at low concentrations [14].

Adsorption is a widely utilized technique generally considered a water-conservative approach that is efficient, applicable on a large scale, and cost-effective for water purification processes. It can be used in dye removal processes where particles are bound to an adsorbent surface by chemical forces (chemisorption) or physical forces (physisorption) [14]. Even though adsorption has numerous benefits, its limitations include finding suitable and cheap adsorbents, and expensive product recovery [15]. To solve this emerging problem, adsorbents obtained from plant and animal waste materials can readily be used due to their low cost, availability, and renewability thereby providing a cheap and efficient process for long-term safe water discharge into the environment [16].

Hydroxyapatite-chitosan (HAP-CS) composite obtained from low-cost, readily available goat bone and periwinkle shell has been identified and used as an adsorbent to remove Indigo Blue (IB) dye from aqueous solution in this study. HAP is white and powdery and is used in fuel-cell materials, fluorescent lights, pollutant adsorption, and catalysis [17]. It can be synthesized chemically or obtained naturally from mammalian bone, marine sources, shell sources, plants and algae, and mineral sources [18]. Despite its advantages, HAP has low porosity, poor stability, and poor mechanical properties, resulting in decreased adsorption properties such as selectivity, capacity, and kinetics [19]. Combining HAP with biopolymers can alleviate these drawbacks. Chitin is a widely used biopolymer for synthesizing HAP composites and is present in shells, cuticles of insects, scales of fish, yeast, and algae. Chitosan (CS) is a biopolymer obtained by partially deacetylating chitin. Due to its availability from renewable sources, low cost, and high activity, it is attractive for adsorption-related processes such as dye and heavy metal removal, and gas capture [20].

This study provides data for the prevention and mitigation of environmental pollutant dye from wastewater using Hydroxyapatite-chitosan composite from agricultural waste (hydroxyapatite obtained from goat bone and chitosan obtained from periwinkle shell). The investigation of the adsorption optimum parameters carried out by RSM will provide data for future processes and its industrial applications.

2.0. Materials and Methods

2.1. Materials

Goat bones and periwinkle shells were sourced locally from a slaughterhouse in Benin City, Edo state, Nigeria. The bones and shells were extensively washed and sun-dried for 5 days. The dry goat bones and periwinkle shells were crushed into smaller particles and processed into fine powder. The powder was sieved to separate particles of approximately 300μm. Analytic grade acetone, hydrochloric acid, sodium hydroxide pellets, acetic acid, and indigo blue dye were purchased from a chemical store in Benin City.

2.2. Composite Synthesis

Hydroxyapatite (HAP) and Chitosan (CS) were prepared using a modified method from the literature [24]. Goat bone char (300 μm) was heated in a muffle furnace from ambient temperature to 800 °C for 3 h, then cooled to obtain HAP. The yield was calculated using Eq 1.

$$\boldsymbol{Y = \frac{W_H}{W_B} \times 100} \quad (1)$$

Where Y represents the HAP yield, W_H and W_B denote the weight of HAP and the bone powder respectively.

Periwinkle shell powder was soaked in 7% (v/v) HCl for 24 h and then in 10% (w/v) NaOH for another 24 h to remove minerals and proteins respectively. It was filtered, washed to a pH of 7, and dried at 90 °C for 1 h [24], [25]. The dried powder was refluxed in acetone for 3 h for decolorization, yielding chitin [26]. The chitin was then treated with 50% (w/v) NaOH for 4 h at 30 °C to obtain CS (2-acetamido-2-deoxy-D-glucose-N-(acetyl glucose amine), which was washed and dried for 1 h at 90 °C [26]. The yield was calculated using Eq 2.

$$Chitosan\ yield = \frac{weight\ of\ chitosan}{weight\ of\ periwinkle\ powder} \times 100 \quad (2)$$

2 % acetic acid was added to the CS and was stirred for 1 h to aid dispersion and bubble removal. The HAP was then added to the CS in a 1:1 ratio and further stirred at ambient temperature for 48 h, before filtration, and drying at 80 °C to obtain the HAP-CS composite.

2.3. Characterization of HAP-CS Composite and Experimental Setup

The FTIR spectrum was captured using a BRUKER model Tensor 27 (Germany) and the KBr disc technique, scanning electron microscopy-energy dispersive X-ray (SEM-EDX, KYKY-EM3200, China) for surface morphology, X-ray diffraction (XRD: Philip X'pert) and X-ray Fluorescence (XRF) for crystallite phase and composition analysis, and BET (Brunauer-Emmett-Teller) analysis was used to measure textural properties. An indigo blue (IB) stock solution of 500 mg L^{-1} was prepared in deionized water, with diluted concentrations (20, 85, and 150 mg L^{-1}) for subsequent tests. The experimental design followed a four-variable Box-Behnken design (BBD) approach with five replications at the middle point using Design Expert® 13.0.0, yielding 29 trials to model the relationship between input variables (time, pH, dye concentration, adsorbent dosage) and removal efficiency. ANOVA was applied to validate model accuracy and the relevance of the coefficients of regression.

Table 1: Levels of the Experimental Factors in the BBD Design.

Variables	Unit	Symbol	Variable coded levels	
			Low level	High level
Time	Minute (min)	A	15	180
pH	-	B	3	11
Dye concentration	mg/L	C	20	150
Adsorbent dosage	g/L	D	1	3

2.4. Experimentals methodology

Adsorption studies were conducted at room temperature with continuous stirring at 180 rpm. Each experiment used the required volume of IB solution and adjusted the initial pH with 0.5 M NaOH or 1 M HCl. Dye concentration was measured at 615.7 nm using a Thermo Scientific Genesys 10S UV-Vis spectrophotometer. Adsorbed dye per gram of adsorbent (q_e) was calculated using Eq. 3

$$q_e = (C_i - C_e)\frac{V}{m} \quad (3)$$

where V (L) is the IB solution volume, C_i (mg L^{-1}) and C_e (mg L^{-1}) represent the initial and equilibrium concentrations respectively, and m (mg) is the adsorbent mass. The percentage removal of IB was given by Eq. 4

$$removal\ \% = (\frac{C_i - C_e}{C_i})\ 100 \quad (4)$$

where C_e and C_i are the equilibrium and initial concentrations (mg L^{-1}).

Freundlich, Langmuir, and Henry isotherm models were applied to assess the adsorption interaction of Indigo Blue on the HAP-CS composite, while the adsorption kinetics of Indigo Blue on HAP-CS were evaluated using pseudo-first-order, pseudo-second-order, and intra-particle diffusion models to study the sorption mechanism and optimize treatment efficiency.

3.0. RESULTS AND DISCUSSION

3.1. Characterization of HAP-CS

SEM-EDX Analysis

The morphology and composition of the HAP-CS composite material pre and post-adsorption studies were captured. Fig 1 shows the surface morphology of the HAP-CS composite before and after the adsorption process. Fig 1(a) shows the morphology of the HAP-CS composite before dye adsorption, revealing a coarse and porous surface, which depicts high adsorptive capacity. These results are similar to those of previous research where HAP-CS composite was used for Remazol Blue Dye (RBD) adsorption [21], indigo dye removal [22], Congo Red (CR) dye adsorption [23], and the removal of brilliant green dye [24]. Fig 1(b) reveals the morphology of the HAP-CS composite after dye adsorption, with clogged pores ascribed to dye adsorption. Fig 2 revealed the EDX analysis of the HAP-CS composite before and after dye adsorption. Fig 2(a) shows the main components; Ca, C, O, and P while Fig 2(b) shows the EDX analysis after dye adsorption, demonstrating compositional modifications and an increase in the amount of C and Na linked to effective dye adsorption onto the HAP-CS composite. These findings are consistent with previous studies on dye removal using HAP-CS composite [25].

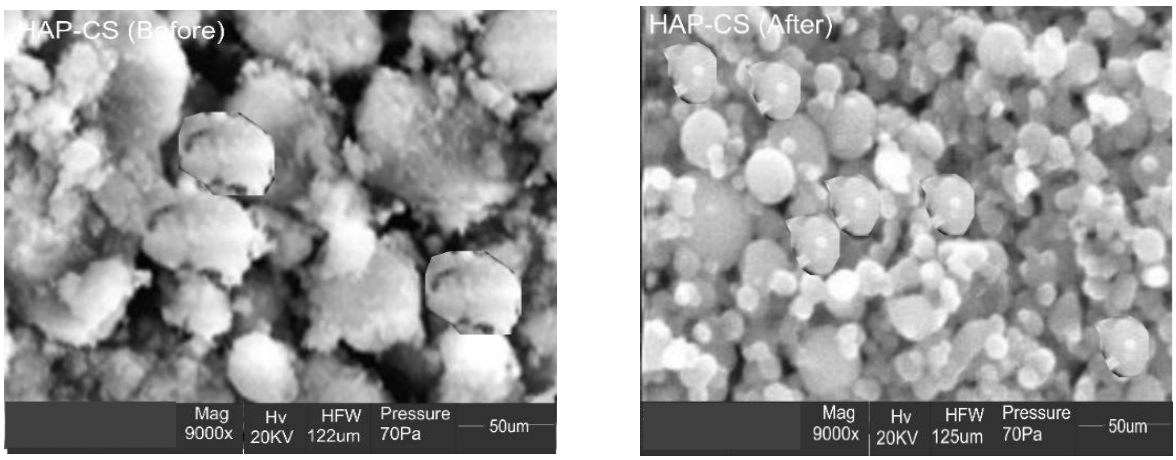

Fig. 1 SEM images of the HAP-CS adsorbent composite (a) before and (b) after adsorption process at ×9000.

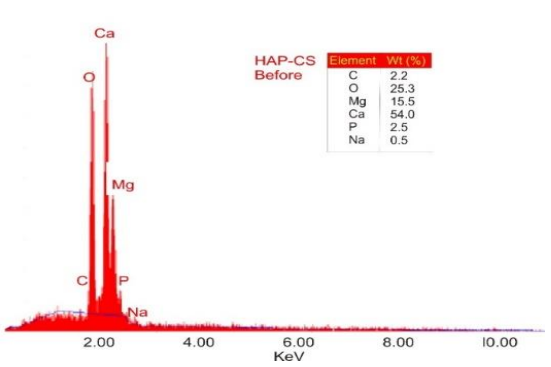

(a)

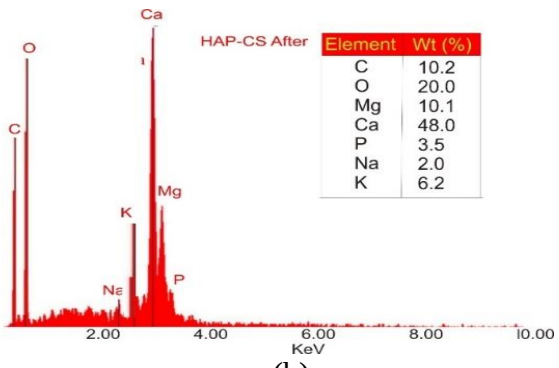

(b)

Fig. 2 The EDX analysis of the HAP-CS adsorbent composite (a) before (b) after the adsorption process.

Textural properties

Adsorption/desorption isotherms were plotted to evaluate the porous structure of the manufactured composite, and they were used to identify morphological traits of the HAP-CS adsorbent composite. Pure HAP had a BET surface area of up to 275.623 m^2g^{-1}, a measured pore volume of 0.136 cc g^{-1}, and a pore diameter of 2.118 nm. The Chitosan (CS) had a BET surface area of up to 331.941 m^2g^{-1}, a measured pore volume of 0.162 cc g^{-1}, and a pore diameter of 2.144 nm. Such high numbers of BET surface area for both the HAP and CS can be ascribed to the excellent crystalline structure of the material [26]. In comparison, the HAP-CS composite adsorbent had a BET surface area of 369.715 m^2g^{-1}, a pore volume of 0.209 cc g^{-1}, and pore diameter of 1.853 nm comparable to previous work [26]. This represents an increase in surface area after combining HAP and CS. Hence, the BET surface areas increased in the order HAP > CS > HAP-CS. The presence of additional pores introduced by chitosan is responsible for the increase in BET surface area as evident from the textural analysis. Chitosan has a porous structure with interconnected void spaces. Hence, when combined with HAP, it produces a composite material with a higher pore volume. These additional pores provide more surface area for adsorption and contribute to the overall BET surface area [27].

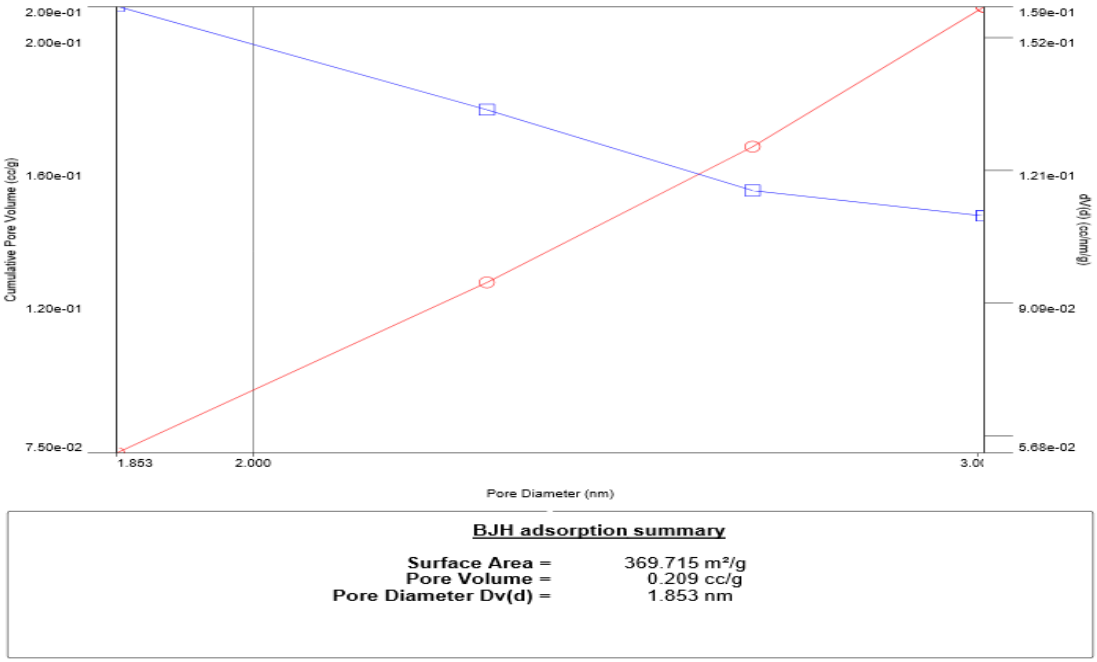

Fig. 3: BJH adsorption summary of HAP-CS adsorbent

X-ray Diffractogram (XRD) Analysis

X-ray diffractogram of the HAP-CS composite depicted in Fig 4, where the HAP crystalline peaks at 2θ = 26.5˚, 32˚, 33 ˚, 33.4 ˚, and 40 ˚ are present with little shifting in 2θ, indicative that the HAP crystallite structure was preserved in the composite. This outcome is consistent with other research [24], [28]furthermore, the HAP-CS composite diffractogram confirmed the crystalline nature of HAP and chitosan powders composite, and the preservation of HAP crystal structure in the HAP-CS composite as reported in literature [29]–[33].

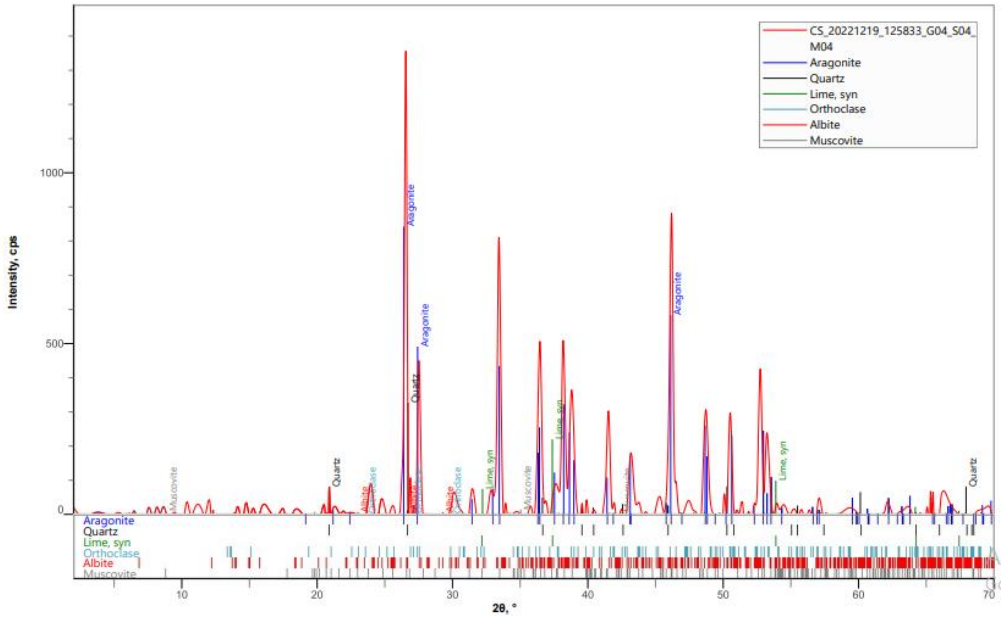

Fig. 4 XRD diffractogram of HAP-CS composite

FTIR Analysis

FTIR spectra of HAP which were obtained in the range of 400- 4000 cm^{-1} represented stretching functional groups. Because of the bending and stretching of PO_4^{-3}, the spectra of HAP displayed a broad band between 450 – 600 cm^{-1} and 1000 - 1150 cm^{-1}. Additionally, P=O stretching vibrations between 1150 and 1350 cm^{-1}, and a matching symmetric stretching was seen between 800 and 1000 cm^{-1} [28]. The large bands at 3200 to 4000 cm^{-1} were ascribed to the O-H groups contained in HAP [25], [28]. Also, the Chitosan powder was subjected to FTIR spectroscopic examination with 4 cm^{-1} resolution and a frequency range of 400 – 4000 cm^{-1}. At wave numbers ranged 3200 – 4000 cm^{-1}, the chitosan's spectrum showed a large broad signal, which is connected to the overlap of the polysaccharide's inter-hydrogen bonds and the overlap of the -OH and $-NH_2$ stretching vibrations [34]. The symmetric and asymmetric $-CH_2$ groups were attributed to peaks in [25], [29].

The FTIR spectrum of the HAP-CS composite adsorbent represented in Fig 5 revealed a band within the range of 1000 - 1250 cm^{-1}, which was caused by the chitosan's C-O-C group's stretching vibration, thereby confirming the synthesis of the adsorbent. Due to the interaction with chitosan, the peak of the $PO4^{3-}$ group shifted. Chitosan's -NH group vibrated in a stretching and bending mode at ranges between 3200 - 4000 cm^{-1}, which overlapped with the O-H groups bands in the HAP-CS adsorbent [28].

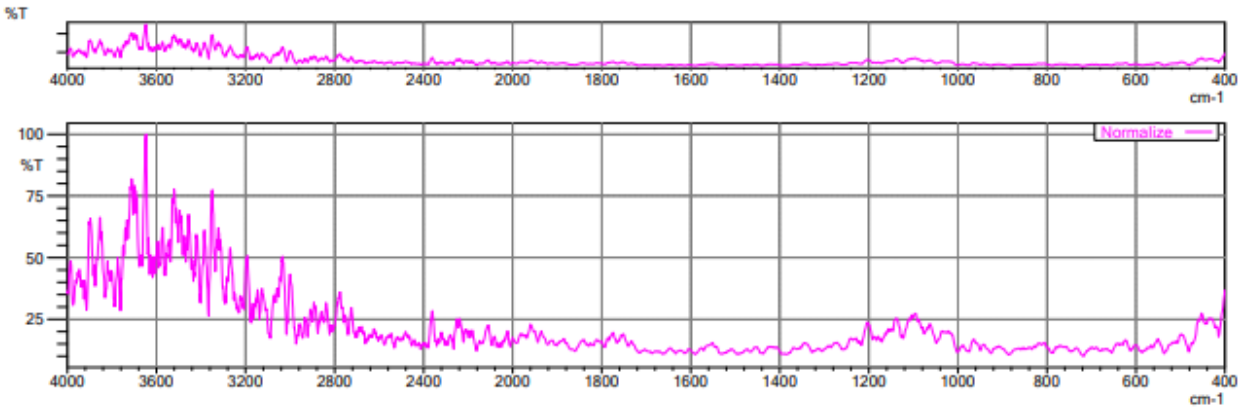

Fig. 5 FTIR analysis of the HAP-CS adsorbent.

XRF Analysis

According to the elemental analysis using XRF, the HAP-CS powders comprised two primary elements, calcium, and phosphorus, which corresponds to the SEM analysis (refer to Fig 1) with additional elements present in trace amounts. Table 2 shows the XRF compositional analysis results of the HAP-CS composite adsorbent. The outcome demonstrated that the HAP-CS composite also had high amounts of CaO and P_2O_5, with concentrations of 68.686 and 25.139 % respectively. The high proportion of CaO and P_2O_5 shows that HAP is potentially rich in calcium and phosphorous which is vital during the synthesis of HAP-CS [35]. The higher adsorption capability of natural hydroxyapatite can be related to the presence of additional trace mineral components [36].

Table 2: XRF analysis of HAP-CS composite adsorbent.

Component	Concentration
SiO_2	1.550
V_2O_5	0.022
Cr_2O_3	0.004
MnO	0.034
Fe_2O_3	0.231
Co_3O_4	0.005
NiO	0.001
CuO	0.028
Nb_2O_3	0.006
MoO_3	0.000
WO_3	0.009
P_20_5	25.139
SO_3	0.052
CaO	68.686
MgO	0.000
K_2O	0.058
BaO	0.156
Al_2O_3	2.543
Ta_2O_5	0.011
T_iO_2	0.027
ZnO	0.014
Ag_2O	0.000
Cl	0.714
ZrO_2	0.062
SnO_2	0.646

3.2. Optimization of Batch Adsorption of Indigo Blue

Fig 6 shows the percentage (%) removal of IB dye on the composite surface as a function of varied contact times with initial concentrations of 80 mg L^{-1}, 1 g of adsorbent, and pH of 3. At these

conditions, the removal rate of the dye by the adsorbent composite surface is 54.29 %. The dye adsorption procedure demonstrated that the adsorption percentage rose significantly and eventually reached equilibrium. The highest removal efficiency was achieved at an optimum adsorption time of 180 min with a small change observed after 120 min. At equilibrium, further treatment was insignificant as all the pore spaces were occupied. The initial high adsorption rate can be attributed to the high BET surface area, leading to more active sites on the outer layer of the adsorbent composite. This explains the initial high adsorption rate resulting from the vacant pores. The adsorbent's porosity also plays a role as evident in the SEM micrographs (refer to Fig1) where the sample revealed small, loosely packed grains with large pores, indicative of the presence of active sites required for an efficient adsorption process [37], [38]. Similar results were reported by Bhowmik et al. [39], where equilibrium was reached at 150 min with a small amount of change after 120 min. Previous studies have also revealed that with an increase in time, the surface of the adsorbent is saturated and unable to continue removing IB dye from the solution [40]. This behaviour is attributed to the high level of interaction between the molecules of the adsorbate and the adsorption sites of the adsorbents [22]. Moreover, at the point of saturation, the repulsive force between the molecules of the dye and the HAP-CS surface attains equilibrium [41].

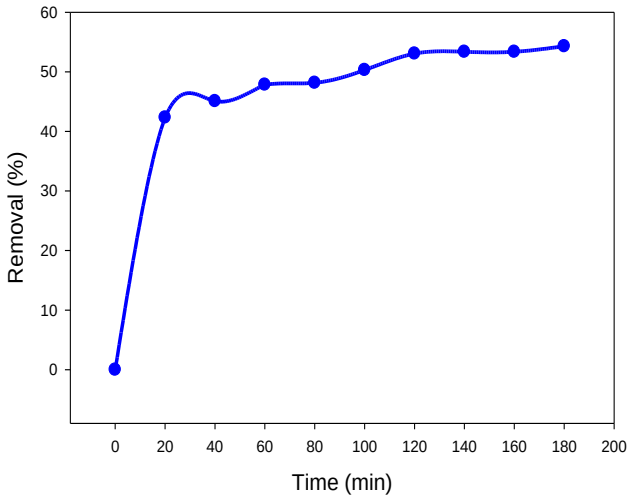

Fig. 6 Effect of time on the adsorption of IB dye

3.3. Isotherm studies

To identify the best fit for this study, Langmuir, Freundlich, and Henry isotherms were compared. Regarding Table 3, the constant K_F in the Freundlich model represents the adsorption capacity while 1/n indicates the heterogeneous nature of the surface [42]. In the Henry isotherm model which has one parameter, linear behaviour of the adsorption process is assumed. According to previous work, the model estimates adsorption capabilities up to a certain value that is typically lower than the saturation value [43], [44]. The Langmuir isotherm model presupposes monolayer coverage with no intermolecular communication among the adsorbed molecules. Additionally, it presupposes that the adsorbent will bind to finite localized sites [45]. Table 4 represents the findings of the Langmuir and Freundlich constants for the IB dye adsorption. The values of K_L and q_m are determined from the slope and intercepts, respectively of the plots of $1/q_e$ versus $1/C_e$ while the values of 1/n and K_F are the slope and intercept, respectively of the graph between $\ln C_e$ versus $\ln q_e$.

The Freundlich isotherm model assumes differential surface energies, while the Langmuir isotherm model presupposes monolayer coverage with no intermolecular communication among the adsorbed molecules. Additionally, it presumes that the adsorbent will adsorb on limited localized areas [45]. Assuming adsorption reversibility and a constant amount of sites accessible for the process derives

the Langmuir isotherm [22]. In this study, the Langmuir model had the best fit with a regression coefficient (R^2) of 0.9683 while the Freundlich isotherm model had a regression coefficient of 0.9333. The Average Relative Error (ARE) of the Langmuir model is 0.89 %. Its isotherm fit is indicative that the synthesized HAP-CS had confined monolayer adsorption with low intermolecular interaction. The non-dimensional separation factor, R_L, (refer to Eq3), was used to assess the favourability of the adsorption process. The R_L formula is given in Eq 5.

$$\boldsymbol{R_L = \frac{1}{1+K_L C_o}} \quad \textbf{(5)}$$

Where, K_L = Langmuir constant, R_L = separation factor, and C_O = initial IB dye concentration.

The separation factor shows the adsorption isotherm to be favourable, linear, or unfavourable when $0 < R_L < 1$, $R_L = 1$, and $R_L > 1$ respectively. The HAP-CS adsorbent had R_L values between 0.87 and 0.95 for the C_O range (50 - 150 mg L^{-1}) employed in the study. Conclusively, this depicts that IB adsorption is preferred on the HAP-CS adsorbent [46]**.**

Table 3: Isotherm models for the HAP-CS adsorption of IB dye [39]

Model	Equation	Parameters
Freundlich isotherm	$q_e = K_F C_e^{1/n}$	K_F = adsorption capacity indicator, 1/n = adsorption intensity indicator
Langmuir isotherm	$\frac{q_e}{q_o} = \frac{K_L C_e}{1 + K_L C_e}$	K_L = Langmuir constant (L/mg), q_o = maximum monolayer coverage (mg/g), q_e = adsorption equilibrium (mg/g), C_e equilibrium concentration (mg/L)
Henry isotherm	$q_e = K_H C_e$	K_H = Henry isotherm constant

Table 4: Results and coefficients of isotherm models

Model	Parameter	R^2	ARE (%)
Freundlich isotherm	K_F = 0.071, n = 1.046	0.9333	2.76
Langmuir isotherm	K_L = 0.001, q_o = 60.241	0.9683	0.89
Henry isotherm	K_H = 0.0494	0.8893	7.35

3.4. Adsorption Kinetic Studies

The IB dye adsorption rate on the HAP-CS surface is shown by the adsorption kinetics models in Eq.(3)-(5) which were employed to fit a model to the obtained data.

$$\ln (q_e - q_t) = \ln(q_e) - k_1 t \quad (6)$$

$$\frac{t}{q_t} = \frac{1}{1+K_2 q_e^2} + \frac{t}{q_e} \quad (7)$$

$$q_t = k_p t^{1/2} + I \quad (8)$$

From the summary of the outcomes represented in Table 5, the pseudo-second-order model had the higher regression coefficient **s**ince it depicts analogous interactions at the surface level [47], and according to literature, dye adsorption typically follows this step. Thus, the data from this study is consistent with the existing research [39], [48]–[50].

Table 5: Values of the kinetic model constants

Models	Constants	Concentration (mg/L)			
		50	80	110	150
Pseudo-first-order	q_e	0.630	1.247	2.891	2.409
	K_1	0.0067	0.0374	0.0249	0.022
	R^2	0.9654	0.9766	0.9951	0.9134
Pseudo-second-order	q_e	3.099	4.088	5.675	10.582
	K_2	0.097	0.049	0.023	0.00743
	R^2	0.9757	0.9869	0.996	0.9239
	I	0.4944	1.7778	2.0323	0.7494

Intraparticle diffusion	K_P	0.154	0.1465	0.2437	0.5488
	R^2	0.9734	0.9631	0.8685	0.9473

3.5. RSM optimization

For analysis, the findings of the adsorption tests performed using the BBD model matrix were employed. The software produced the following model depicted as Eq. 9

$$\textbf{Removal efficiency (\%)} = +61.04 + 11.59A + 2.55B + 13.67C + 6.60D - 14.13AB - 5.60AC - 3.98AD + 4.11BC + 8.01BD - 6.70CD - 4.08A^2 + 0.8594B^2 - 14.58\,C^2 + 1.06D^2 \quad (9)$$

Fig. 7 presents a visual comparison of the model's predicted values and experimental data. Statistical analysis using ANOVA revealed the quadratic model's significance, supported by a substantial Fisher's F-value (16.61) and a highly significant probability value ($P < 0.0001$) [51]. Detailed results are summarized in Table 6

Table 6 ANOVA data for the optimization process

Source	Sum of Squares	df	Mean Square	F-value	p-value	
Model	7666.78	14	547.63	67.44	< 0.0001	significant
A-Time	4936.15	1	4936.15	607.87	< 0.0001	
B-pH	0.8802	1	0.8802	0.1084	0.7469	
C-Dye concentration	2567.86	1	2567.86	316.22	< 0.0001	
D-Adsorbent dosage	19.13	1	19.13	2.36	0.1471	
AB	0.5402	1	0.5402	0.0665	0.8002	
AC	8.18	1	8.18	1.01	0.3326	
AD	0.0272	1	0.0272	0.0034	0.9546	
BC	14.21	1	14.21	1.75	0.2070	
BD	6.50	1	6.50	0.8008	0.3860	
CD	21.90	1	21.90	2.70	0.1228	
A^2	2.61	1	2.61	0.3218	0.5795	
B^2	0.0112	1	0.0112	0.0014	0.9709	
C^2	24.30	1	24.30	2.99	0.1057	
D^2	62.70	1	62.70	7.72	0.0148	
Residual	113.69	14	8.12			
Lack of Fit	106.43	10	10.64	5.86	0.0515	Not significant
Pure Error	7.26	4	1.81			
Cor Total	7780.47	28				

The regression model's statistical significance was suggested by its high R^2 value (0.9432). According to Table 7, the adjusted R^2 value was 0.8864, while the projected R^2 value was 0.7624, which relatively agreed with the adjusted R^2. A signal was sufficient when the signal-to-noise ratio was 16.981 (>4), and a 10.51 % coefficient of variance was discovered. Hence, the ANOVA analysis showed the model's suitability for removing dye using HAP-CS adsorbent within the experimental range.

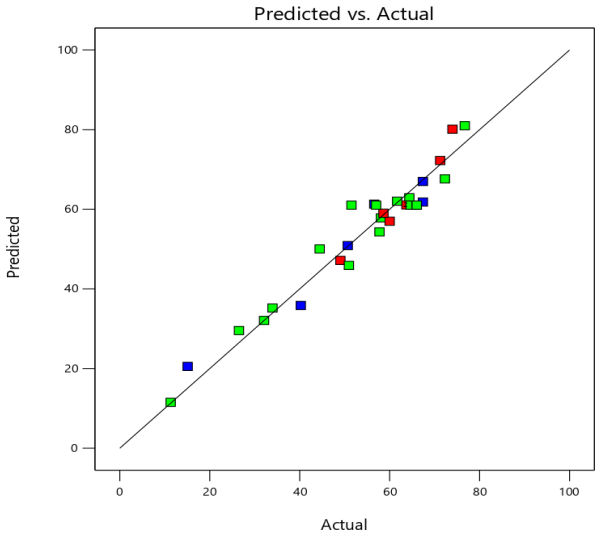

Fig. 7. Predicted vs actual values of IB removal efficiency using HAP-CS as adsorbent

Table 7: RSM model statistics of goodness of fit

Parameter	Value
R^2	0.9854
Adjusted R^2	0.9708
Predicted R^2	0.9198
Adeq Precision	34.0679
Std. Dev.	2.85
Mean	47.98
C.V. %	5.94

The interactions of the parameters during the sorption of the Indigo Blue dye were studied using the contour plots as a function of two elements while keeping the other components at the central level. The red colour denotes a higher removal percentage. Red's transition into yellow and green shows a lesser degree of elimination. **Error! Reference source not found.**(a) illustrates the pH and dosage effects on removal effectiveness. An increase in removal effectiveness is recorded when the dose and time are increased. **Error! Reference source not found.** (b) shows the effect of pH and contact time on removal efficiency. A lower pH and longer contact time produced an increased efficiency. The responses of the dye concentration and contact time on the removal efficiency were analysed and are depicted in **Error! Reference source not found.** (c). The model's findings for the optimum conditions were: pH = 3, time = 180 min, adsorbent dosage = 2 g, and dye concentration = 85 mg L^{-1}. The computed removal efficiency under these circumstances was 81 %. The experimental value attained under these circumstances was 76.71 %, which is relatively close to the expected value (relative error: 4.29 %).

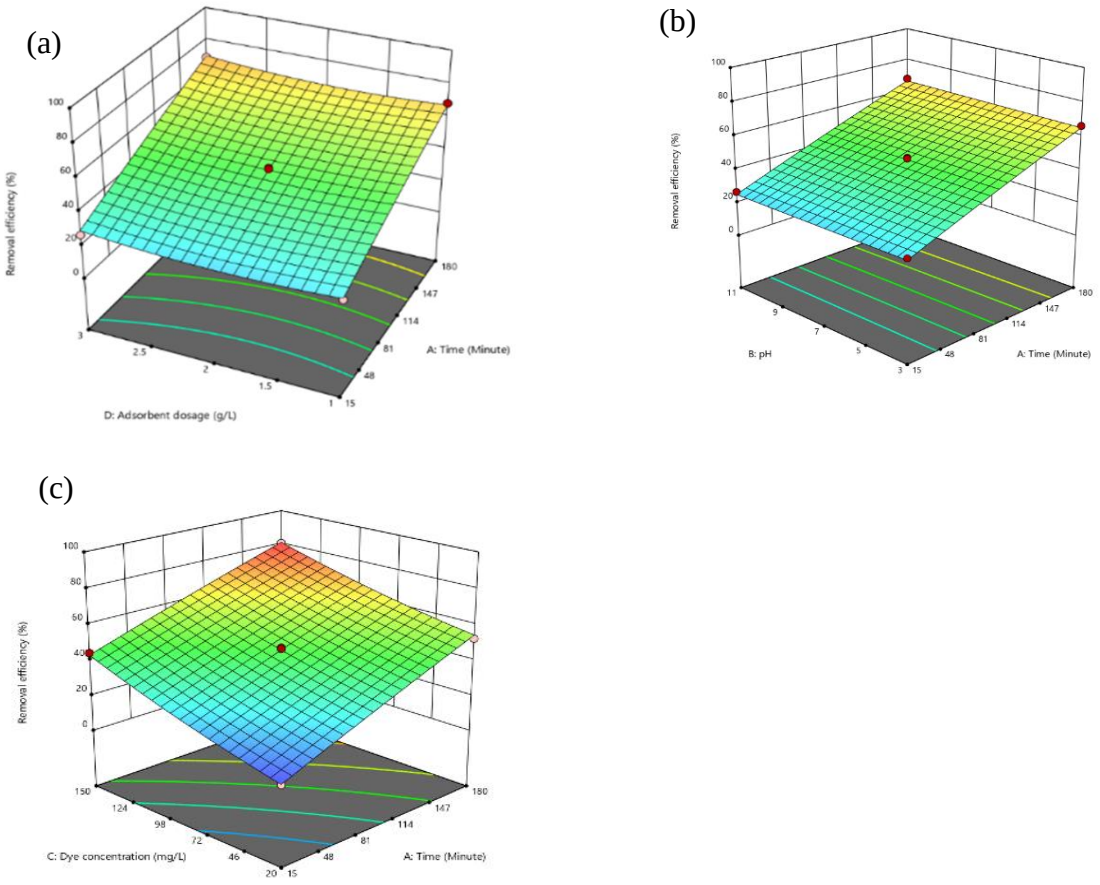

Fig. 8. (a) Effect of dosage and time on removal efficiency of IB dye using HAP-CS as adsorbent, (b) Effect of contact time and pH on removal efficiency of IB using HAP-CS as adsorbent and (c) Effect of dye concentration and time on removal efficiency of IB using HAP-CS as adsorbent.

4. Conclusions

This study investigated the use of a composite hydroxyapatite-chitosan (HAP-CS) adsorbent to remove Indigo Blue dye from an aqueous solution. The HAP-CS adsorbent is synthesized from waste materials; hence it is an affordable and practical wastewater treatment option. The ideal parameters for the adsorption process were found using the Box-Behnken design by examining the effects of pH, dye concentration, and adsorbent dosage on the efficacy of adsorption using the experimental design. Further optimisation of the process parameters was achieved by using the response surface methodology (RSM) model. The HAP-CS composite effectively removed the Indigo Blue dye from the aqueous solution with a high adsorption efficiency of 80.92 %. This suggests HAP-CS composite could be a suitable candidate for treating wastewater, particularly in removing textile dyes. Overall, the promising potential of the HAP-CS composite adsorbent synthesized from low-cost waste materials has been reported. Its successful adsorption of Indigo Blue dye from aqueous solutions highlights its applicability in wastewater treatment applications. The study also underlined the importance of employing advanced modelling techniques like RSM to optimize adsorption processes and enhance the efficiency of wastewater treatment systems.

References

[1] P. Senthil Kumar and P. R. Yaashikaa, “Introduction—Water,” *Water Text. Fash.*, pp. 1–20, Jan. 2019.
[2] P. Li, D. Karunanidhi, T. Subramani, and K. Srinivasamoorthy, “Sources and Consequences of Groundwater Contamination,” *Arch. Environ. Contam. Toxicol.*, vol. 80, no. 1, pp. 1–10, Jan. 2021.

[3] K. Obaideen, N. Shehata, E. T. Sayed, M. A. Abdelkareem, M. S. Mahmoud, and A. G. Olabi, "The role of wastewater treatment in achieving sustainable development goals (SDGs) and sustainability guideline," *Energy Nexus*, vol. 7, p. 100112, Sep. 2022.

[4] L. Schweitzer and J. Noblet, "Water Contamination and Pollution," *Green Chem. An Incl. Approach*, pp. 261–290, Jan. 2018.

[5] U. Nimkar, "Sustainable chemistry: A solution to the textile industry in a developing world," *Curr. Opin. Green Sustain. Chem.*, vol. 9, pp. 13–17, Feb. 2018.

[6] O. A. Oguntade, J. O. Azeez, T. Arowolo, and F. K. Salako, "Tertiary Education Trust Fund View project maize production View project," 2018.

[7] J. Dotto, M. R. Fagundes-Klen, M. T. Veit, S. M. Palácio, and R. Bergamasco, "Performance of different coagulants in the coagulation/flocculation process of textile wastewater," *J. Clean. Prod.*, vol. 208, pp. 656–665, Jan. 2019.

[8] V. Bharti *et al.*, "Biodegradation of methylene blue dye in a batch and continuous mode using biochar as packing media," *Environ. Res.*, vol. 171, pp. 356–364, Apr. 2019.

[9] M. S. Anantha *et al.*, "Comparison of the photocatalytic, adsorption and electrochemical methods for the removal of cationic dyes from aqueous solutions," *Environ. Technol. Innov.*, vol. 17, p. 100612, Feb. 2020.

[10] J. Joseph, R. C. Radhakrishnan, J. K. Johnson, S. P. Joy, and J. Thomas, "Ion-exchange mediated removal of cationic dye-stuffs from water using ammonium phosphomolybdate," *Mater. Chem. Phys.*, vol. 242, p. 122488, Feb. 2020.

[11] M. Naushad, A. A. Alqadami, Z. A. AlOthman, I. H. Alsohaimi, M. S. Algamdi, and A. M. Aldawsari, "Adsorption kinetics, isotherm and reusability studies for the removal of cationic dye from aqueous medium using arginine modified activated carbon," *J. Mol. Liq.*, vol. 293, p. 111442, Nov. 2019.

[12] J. Jiao, J. Zhao, and Y. Pei, "Adsorption of Co(II) from aqueous solutions by water treatment residuals," *J. Environ. Sci.*, vol. 52, pp. 232–239, Feb. 2017.

[13] Y. Zhou, J. Lu, Y. Zhou, and Y. Liu, "Recent advances for dyes removal using novel adsorbents: A review," *Environ. Pollut.*, vol. 252, pp. 352–365, Sep. 2019.

[14] S. Pai, M. S. Kini, and R. Selvaraj, "A review on adsorptive removal of dyes from wastewater by hydroxyapatite nanocomposites," *Environ. Sci. Pollut. Res. 2019 2810*, vol. 28, no. 10, pp. 11835–11849, Dec. 2019.

[15] V. Katheresan, J. Kansedo, and S. Y. Lau, "Efficiency of various recent wastewater dye removal methods: A review," *J. Environ. Chem. Eng.*, vol. 6, no. 4, pp. 4676–4697, Aug. 2018.

[16] Y. Dai *et al.*, "Utilizations of agricultural waste as adsorbent for the removal of contaminants: A review," *Chemosphere*, vol. 211, pp. 235–253, Nov. 2018.

[17] A. Fihri, C. Len, R. S. Varma, and A. Solhy, "Hydroxyapatite: A review of syntheses, structure and applications in heterogeneous catalysis," *Coord. Chem. Rev.*, vol. 347, pp. 48–76, Sep. 2017.

[18] N. A. S. Mohd Pu'ad, P. Koshy, H. Z. Abdullah, M. I. Idris, and T. C. Lee, "Syntheses of hydroxyapatite from natural sources," *Heliyon*, vol. 5, no. 5, May 2019.

[19] A. Nayak and B. Bhushan, "Hydroxyapatite as an advanced adsorbent for removal of heavy metal ions from water: Focus on its applications and limitations," *Mater. Today Proc.*, vol. 46, pp. 11029–11034, Jan. 2021.

[20] X. qi Liu, X. xin Zhao, Y. Liu, and T. an Zhang, "Review on preparation and adsorption properties of chitosan and chitosan composites," *Polym. Bull. 2021 794*, vol. 79, no. 4, pp. 2633–2665, Mar. 2021.

[21] S. Hamzah and M. F. M. Salleh, "Hydroxyapatite/ Chitosan Biocomposite for Remazol Blue Dyes Removal," *Appl. Mech. Mater.*, vol. 695, pp. 106–109, Nov. 2015.

[22] A. A. Okoya and D. Diisu, "Adsorption of Indigo-dye from Textile Wastewater onto Activated Carbon Prepared from Sawdust and Periwinkle Shell," *Trends Appl. Sci. Res.*, vol. 16, no. 1, pp. 1–9, 2021.

[23] H. Hou, R. Zhou, P. Wu, and L. Wu, "Removal of Congo red dye from aqueous solution with hydroxyapatite/chitosan composite," *Chem. Eng. J.*, vol. 211–212, pp. 336–342, Nov. 2012.

[24] A. Ragab, I. Ahmed, and D. Bader, "The Removal of Brilliant Green Dye from Aqueous Solution Using Nano Hydroxyapatite/Chitosan Composite as a Sorbent," *Mol. 2019, Vol. 24, Page 847*, vol. 24, no. 5, p. 847, Feb. 2019.

[25] M. Rastgordani and J. Zolgharnein, "Simultaneous Determination and Optimization of Titan Yellow and Reactive Blue 4 Dyes Removal Using Chitosan@hydroxyapatite Nanocomposites," *J. Polym. Environ.*, vol. 29, no. 6, pp. 1789–1807, Jun. 2021.

[26] T. Szatkowski *et al.*, "Synthesis and characterization of hydroxyapatite/chitosan composites," *Physicochem. Probl. Miner. Process.*, vol. 51, no. 2, pp. 575–585, 2015.

[27] T. Başargan and G. Nasün-Saygılı, "Spray-Dried Mesoporous Hydroxyapatite–Chitosan Biocomposites," *Polym. Plast. Technol. Eng.*, vol. 54, no. 11, pp. 1172–1183, Aug. 2015.

[28] N. Gupta, A. K. Kushwaha, and M. C. Chattopadhyaya, "Adsorptive removal of Pb 2+, Co 2+ and Ni 2+ by hydroxyapatite/chitosan composite from aqueous solution," *J. Taiwan Inst. Chem. Eng.*, vol. 43, no. 1, pp. 125–131, 2012.

[29] K. S. Abdullah Al Balushi, G. Devi, A. S. Rashid Khamis Al Gharibi, M. A. S. Adeeb, A. S. M. Al Hudaifi, and S. S. Khalfan Al Shabibi, "Extraction of bio polymers from crustacean shells and its application in refinery

wastewater treatment," *Walailak J. Sci. Technol.*, vol. 18, no. 5, pp. 1–11, 2021.

[30] M. T. Yen, J. H. Yang, and J. L. Mau, "Physicochemical characterization of chitin and chitosan from crab shells," *Carbohydr. Polym.*, vol. 75, no. 1, pp. 15–21, 2009.

[31] R. A. A. Muzzarelli *et al.*, "Chitin nanofibrils/chitosan glycolate composites as wound medicaments," *Carbohydr. Polym.*, vol. 70, no. 3, pp. 274–284, 2007.

[32] N. Méndez-Lozano *et al.*, "Crystal growth and structural analysis of hydroxyapatite nanofibers synthesized by the hydrothermal microwave-assisted method," *Ceram. Int.*, vol. 43, no. 1, pp. 451–457, Jan. 2017.

[33] R. Barabás, M. Czikó, I. Dékány, L. Bizo, and E. S. Bogya, "Comparative study of particle size analysis of hydroxyapatite-based nanomaterials," *Chem. Pap.*, vol. 67, no. 11, pp. 1414–1423, Nov. 2013.

[34] Z. A. Sutirman, M. M. Sanagi, K. J. Abd Karim, W. A. Wan Ibrahim, and B. H. Jume, "Equilibrium, kinetic and mechanism studies of Cu(II) and Cd(II) ions adsorption by modified chitosan beads," *Int. J. Biol. Macromol.*, vol. 116, pp. 255–263, Sep. 2018.

[35] P. H. Yanti and R. Pebrianti, "Microwave-assisted of synthesis and characterization of nanocomposite hydroxyapatite-chitosan," *J. Phys. Conf. Ser.*, vol. 1842, no. 1, 2021.

[36] A. Ghedjemis, R. Ayeche, A. Benouadah, and N. Fenineche, "A new application of Hydroxyapatite extracted from dromedary bone: Adsorptive removal of Congo red from aqueous solution," *Int. J. Appl. Ceram. Technol.*, vol. 18, no. 3, pp. 590–597, May 2021.

[37] J. K. Abifarin, D. O. Obada, E. T. Dauda, and D. Dodoo-Arhin, "Experimental data on the characterization of hydroxyapatite synthesized from biowastes," *Data Br.*, vol. 26, p. 104485, Oct. 2019.

[38] T. S. Trung *et al.*, "Valorization of fish and shrimp wastes to nano-hydroxyapatite/chitosan biocomposite for wastewater treatment," *J. Sci. Adv. Mater. Devices*, vol. 7, no. 4, p. 100485, Dec. 2022.

[39] S. Bhowmik, V. Chakraborty, and P. Das, "Batch adsorption of indigo carmine on activated carbon prepared from sawdust: A comparative study and optimization of operating conditions using Response Surface Methodology," *Results in Surfaces and Interfaces*, vol. 3, p. 100011, May 2021.

[40] Z. Harrache, M. Abbas, T. Aksil, and M. Trari, "Thermodynamic and kinetics studies on adsorption of Indigo Carmine from aqueous solution by activated carbon," *Microchem. J.*, vol. 144, pp. 180–189, Jan. 2019.

[41] S. Banerjee and M. C. Chattopadhyaya, "Adsorption characteristics for the removal of a toxic dye, tartrazine from aqueous solutions by a low cost agricultural by-product," *Arab. J. Chem.*, vol. 10, pp. S1629–S1638, May 2017.

[42] J. O. Ojediran, A. O. Dada, S. O. Aniyi, and R. O. David, "Functionalized Zea Mays Cob (FZMC) as low-cost agrowaste for effective adsorption of malachite green dyes data set," *Chem. Data Collect.*, vol. 30, p. 100563, Dec. 2020.

[43] M. A. Ahmadi and S. R. Shadizadeh, "Induced effect of adding nano silica on adsorption of a natural surfactant onto sandstone rock: Experimental and theoretical study," *J. Pet. Sci. Eng.*, vol. 112, pp. 239–247, Dec. 2013.

[44] N. Ayawei, A. N. Ebelegi, and D. Wankasi, "Modelling and Interpretation of Adsorption Isotherms," *J. Chem.*, vol. 2017, 2017.

[45] A. O. Dada *et al.*, "Sustainable and low-cost Ocimum gratissimum for biosorption of indigo carmine dye: kinetics, isotherm, and thermodynamic studies," *https://doi.org/10.1080/15226514.2020.1785389*, pp. 1524–1537, 2020.

[46] V. Chakraborty, P. Das, and P. K. Roy, "Carbonaceous materials synthesized from thermally treated waste materials and its application for the treatment of Strontium metal solution: Batch and optimization using Response Surface Methodology," *Environ. Technol. Innov.*, vol. 15, p. 100394, Aug. 2019.

[47] H. N. Tran, Y. F. Wang, S. J. You, and H. P. Chao, "Insights into the mechanism of cationic dye adsorption on activated charcoal: The importance of π–π interactions," *Process Saf. Environ. Prot.*, vol. 107, pp. 168–180, Apr. 2017.

[48] T. Patra, A. Mohanty, L. Singh, S. Muduli, P. K. Parhi, and T. R. Sahoo, "Effect of calcination temperature on morphology and phase transformation of MnO2 nanoparticles: A step towards green synthesis for reactive dye adsorption," *Chemosphere*, vol. 288, p. 132472, Feb. 2022.

[49] J. El Gaayda *et al.*, "Removal of cationic dye from coloured water by adsorption onto hematite-humic acid composite: Experimental and theoretical studies," *Sep. Purif. Technol.*, vol. 288, p. 120607, May 2022.

[50] L. C. Paredes-Quevedo, C. González-Caicedo, J. A. Torres-Luna, and J. G. Carriazo, "Removal of a Textile Azo-Dye (Basic Red 46) in Water by Efficient Adsorption on a Natural Clay," *Water. Air. Soil Pollut.*, vol. 232, no. 1, pp. 1–19, Jan. 2021.

[51] K. Sinha, P. Das Saha, and S. Datta, "Extraction of natural dye from petals of Flame of forest (Butea monosperma) flower: Process optimization using response surface methodology (RSM)," *Dye. Pigment.*, vol. 94, no. 2, pp. 212–216, Aug. 2012.